



DOI: 10.29026/oea.2020.190037

Development of a hybrid photoacoustic and optical monitoring system for the study of laser ablation processes upon the removal of encrustation from stonework

Athanasia Papanikolaou^{1,2†}, George J. Tserevelakis^{1†},
Kristalia Melessanaki¹, Costas Fotakis^{1,2}, Giannis Zacharakis^{1*} and
Paraskevi Pouli^{1*}

In the context of this work, a prototype hybrid photoacoustic (PA) and optical system for the on-line monitoring of laser cleaning procedures is presented. The developed apparatus has enabled the detection of MHz frequency range acoustic waves generated during the laser ablation process. The intrinsically generated PA signals combined with high resolution optical images provide the opportunity to follow the cleaning process accurately and in real time. Technical mock-ups have been used to demonstrate the potential of this novel technique with emphasis given to applications that refer to the restoration of Cultural Heritage (CH) surfaces. Towards this purpose, the real time monitoring of the laser assisted removal of unwanted encrustation from stonework has been achieved using IR and UV wavelengths. This novel approach has allowed for the precise determination of the critical number of laser pulses required for the elimination of the encrustation layer, while highlighting the dominant ablation mechanisms according to the irradiation wavelength. The promising results obtained using the prototype hybrid PA and optical system can open up new perspectives in the monitoring of laser cleaning interventions, promoting an improved restoration outcome.

Keywords: photoacoustic monitoring; laser cleaning; encrusted marble; real time monitoring; two-wavelengths cleaning

Papanikolaou A, Tserevelakis G J, Melessanaki K, Fotakis C, Zacharakis G et al. Development of a hybrid photoacoustic and optical monitoring system for the study of laser ablation processes upon the removal of encrustation from stonework. *Opto-Electron Adv* **3**, 190037 (2020).

Introduction

Laser assisted removal of unwanted material from artworks has been established as a highly precise and safe restoration intervention in the last decades, often substituting conventional cleaning methods. Lasers, due to their unique properties, offer a number of exceptional attributes that allow for selective, gradual, well-defined and precisely controlled material removal, while the production of byproducts is minimal compared to conven-

tional cleaning methods based on chemicals or abrasives. Laser cleaning relies on the ablation of a material upon its irradiation with an intense and short-pulse laser beam at a wavelength that is strongly absorbed by this material^{1,2}. It is a delicate and irreversible process which, due to the exceptionally complex nature of the deposition layers and the, often fragile, condition of the original artworks' surface, requires careful selection of the irradiation parameters (i.e. laser wavelength, fluence values, number of applied pulses, pulse duration, repetition rate etc.)³⁻⁵. For

¹Foundation for Research and Technology Hellas, Institute of Electronic Structure and Laser, N. Plastira 100, Heraklion, Crete 70013, Greece.

²Department of Physics, University of Crete, Voutes University Campus, Crete 71003, Greece.

[†]These authors contributed equally to this work.

*Correspondence: P Pouli, E-mail: ppouli@iesl.forth.gr; G Zacharakis, E-mail: zahari@iesl.forth.gr

Received: 27 September 2019; Accepted: 5 November 2019; Published: 22 February 2020

example, damage of the substrate may occur as a result of overexposure to high fluence values or excessive number of pulses. On the other hand, residues and discoloration may be observed, if the employed fluence or the number of pulses is not adequate for the total elimination of the crust. Along these lines, significant research efforts have been dedicated to the optimization of the laser parameters and the cleaning process, as well as, the monitoring of the ablation progress through micro or non-destructive analytical and diagnostic techniques.

The reliable assessment of the cleaning result in-situ has been investigated using a variety of cutting-edge analytical techniques, most of the times with encouraging results^{2,6-20}. Nevertheless, the on-line and real time monitoring of the laser cleaning progress remains a critical open issue that attracts the interest of the scientific community working in the field of heritage science. The development of a robust diagnostic technique that will follow the cleaning progress in-situ, in real time and will be able to give input on critical levels allowing thus the conservator/restorer to decide on the next steps is a highly challenging task. In this respect, the sensitivity of the technique as regards the physicochemical properties change of the involved materials, the geometry of the object to be cleaned, the time necessary for the assessment of the recorded data, the required spatiotemporal resolution, as well as, the portability and cost of the experimental equipment are particularly important parameters. Laser induced breakdown spectroscopy (LIBS)^{2,6-11}, laser induced fluorescence (LIF)^{7,11,12}, multispectral and hyperspectral imaging¹³⁻¹⁵, speckle imaging¹⁶, digital holographic speckle interferometry^{17,18} and optical coherence tomography (OCT)^{19,20} are some of the analytical techniques that have been considered for the effective assessment of the treated surfaces, as well as, the in-situ evaluation of the cleaning progress. In all these studies the final aim was to monitor in real time the laser restoration interventions in a variety of applications, such as the removal of environmental crust from stone, the cleaning of salts and other deposits from wall paintings, and the elimination of aged varnish from wooden artefacts and easel paintings.

In this respect, photoacoustic (PA) diagnostic approaches have been investigated as regards their potentials to reliably monitor laser cleaning interventions²²⁻²⁸. The fundamental concept behind such techniques is the measurement and recording of acoustic waves inherently generated following the absorption of intensi-

ty-modulated (e.g. pulsed) light by a material, in order to extract valuable information on the cleaning progress. As a matter of fact, upon the interaction of a pulsed laser beam with a material, the absorbed light is converted into thermal energy through non-radiative de-excitation processes, resulting into a local temperature rise of the interacting medium. This temperature change is subsequently followed by a rapid thermoelastic expansion of the medium, leading finally to the generation of an initial pressure. This propagates in space in the form of acoustic waves and can be recorded through appropriate detectors such as microphones or piezoelectric sensors²¹. Several research efforts have been dedicated to the use of the PA effect for the monitoring of laser cleaning procedures using either conventional microphones or ultrasonic transducers with central frequencies in the MHz regime. The gradual material removal can be monitored through variations of the PA amplitude, attributed mainly to the different inherent optical absorption properties between the unwanted over layer and the underlying material.

One of the first attempts to monitor the cleaning progress using the sound generated during the ablation, was introduced by Copper et al.²², in an effort to evaluate the selective removal of black crusts from polluted limestone. In their work, the authors demonstrated that the amplitude of the generated PA signal can be used as a measure of the material removal and confirmed the advantages of wet cleaning, using a Q-Switched (QS) Nd:YAG laser at 1064 nm and a dynamic coil microphone with a frequency response between 100 Hz and 12 kHz (audible frequencies). Lee et al.²³ has reported the successful monitoring of laser cleaning procedures using a microphone in frequencies ranging from 10 Hz up to 15 kHz and, again, a QS Nd:YAG laser for a variety of materials such as marble, copper and paper. The research aim was to investigate the magnitude of the generated acoustic waves and correlate them to the evolution and evaluation of the cleaning progress. In this work, the possibility of the automation of the cleaning using neural network approaches was introduced and discussed. Later, Bregar et al.²⁴, monitored the removal of paint films from stainless steel, glass and marble using a XeCl laser emitting at 308 nm. For monitoring purposes, a multiple-pass laser beam deflection probe technique for the detection of the PA signal in the 10 MHz regime was followed. Similarly, Jankowska et al.²⁵ examined the acoustic effect for the monitoring of black crust removal from sandstone using a QS Nd:YAG laser at 1064 nm and 532 nm. In this publication the authors

associated the exponential signal decay with the decreasing thickness of the crust. The PA technique has been also employed by Gómez et al.²⁶ for the determination of the ablation thresholds of commercial graffiti sprays using lasers emitting at 1064 nm and 308 nm. In another relevant study, Villareal-Villela et al.²⁷ introduced the fast Fourier transform (FFT) of the acquired signal in the context of a photoacoustic induced by laser ablation (PILA) technique for the monitoring of laser assisted paint removal from metallic surfaces. The authors studied the amplitude of the signal and the magnitude of the FFT for the evaluation of the cleaning progress using a QS Cr:YAG laser at 1064 nm. Finally, in a recent research, Tserevelakis et al.²⁸ applied the PA technique for the monitoring of laser cleaning of commercial black graffiti from marble. In this work, a QS Nd:YAG laser at 1064 nm and a piezoelectric contact transducer with a central frequency at 5 MHz were used to investigate the outcome of different irradiation conditions for varying fluence values. Following this approach, a statistical methodology aiming to detect the onsets regarding the paint ablation, efficient cleaning and damage induced to the marble during the laser cleaning process was developed and optimized.

In the present study, the development of a prototype hybrid photoacoustic (PA) and optical system dedicated to the on-line and real time monitoring of pulsed laser cleaning interventions is presented. To demonstrate the capabilities of this approach, a common laser cleaning case has been selected: the removal of pollution encrustation from stonework. The laser assisted removal of dark pollution crusts from stone substrates is one of the first cleaning challenges that have been effectively faced in the laser cleaning research. Such crusts are often developed on the surface of monuments exposed to urban environment due to the microclimate, acid rain, humidity and airborne particles^{29,30}. In an effort to remove the crust from the surface of the marble, while respecting protective layers such as patinas, IR lasers have been used. However, the irradiated surfaces often appeared discolored to yellow hues which is an undesirable side effect^{4,31}. The yellowing or discoloration effect has been extensively studied and a number of hypotheses regarding its exact origin have been formulated through the last years^{32–37}. One of the methodologies developed to overcome this issue was the simultaneous use of two laser beams emitted from a single laser system^{4,5,34,35,37} in order to remove effectively the encrustation without changes of the color, chemistry or structure of the underlying marble. The ef-

fectiveness of this methodology relies on the combination of IR and UV radiation, at a specific ratio and respective fluence values, in an effort to modulate the different ablation mechanisms, thus providing an optimal cleaning result. The combination of the two beams removes dark colored particles and organic compounds along with the material that composes the matrix of the crust (mainly gypsum) at the same time, resulting thus into a homogeneous and efficient cleaning procedure^{4,28,29}.

In our experiments, the developed hybrid setup has been used for the monitoring of cleaning tests performed on simplified mock-ups of marble with simulation of environmental encrustation, highlighting additionally important information regarding the dominant ablation mechanisms upon irradiation using either single IR and, UV laser beams or their respective combinations.

Materials and methods

Mock-up preparation

A commercial marble variety (Thassos White), commonly encountered in Greece, was used for our experiments. It is a pure white, medium to coarse grained marble, with visible grains. The mineralogical composition is 12% Calcite (CaCO_3), 86% Dolomite ($\text{CaMg}(\text{CO}_3)_2$) and 2% Quartz (SiO_2). Slabs of 14 cm \times 7 cm \times 1 cm were used for the performed cleaning tests. The marble slabs were covered with a simplified simulation of environmental crust in layers of varying thickness, ranging from 50 μm up to 150 μm . The crust simulation was a mixture of gypsum with 5% w/w carbon in the form of charcoal particles⁴. The gypsum was in the form of pure hemihydrate provided by a chemical company (95% purity Sigma Aldrich), while the carbon was provided by Fluka Chemica. The mixture was hydrated using distilled water while the mock-ups were left to dry for at least 48 hours prior to any experiment.

Laser system and parameters

The system used for the laser cleaning trials was a BMI Q-switched Nd:YAG system (5022 DNS10 series, B.M. Industries, France) modified by IESL-FORTH to operate at the fundamental (1064 nm) and the third harmonic (355 nm) wavelengths individually and simultaneously^{4,5,35}. The pulse width was 6.5 ns and the repetition rate used was 1 Hz. The laser beams were focused to various spot sizes in the range of approximately 2 mm \times 3 mm as measured on black areas of a printed black and white photographic paper. All irradiation tests were performed

in dry conditions. The mock-ups were placed on an automated XY system (8MT160-300, Standa, Vilnius, Lithuania) which enabled the regulation of their positioning using custom developed software.

Hybrid photoacoustic and optical monitoring system

The developed apparatus was used to record the intrinsically generated PA waves and a monochromatic optical image in synchronization with every incident laser pulse (Fig. 1). PA signals were detected using a contact piezoelectric transducer (C110-RM Centrascan, Olympus, Japan; central frequency: 5 MHz, 0.25-inch element diameter) fixed at the corner of the mock-up and were amplified using a low noise and high sensitivity RF amplifier (AU-1291, Miteq, USA; gain: 63 dB). The signal was subsequently digitized by a high-speed oscilloscope (DSO7034A, Agilent Technologies, USA; bandwidth 350 MHz, maximum sample rate 2GSamples/sec), which is synchronized with the laser trigger and finally recorded by a computer.

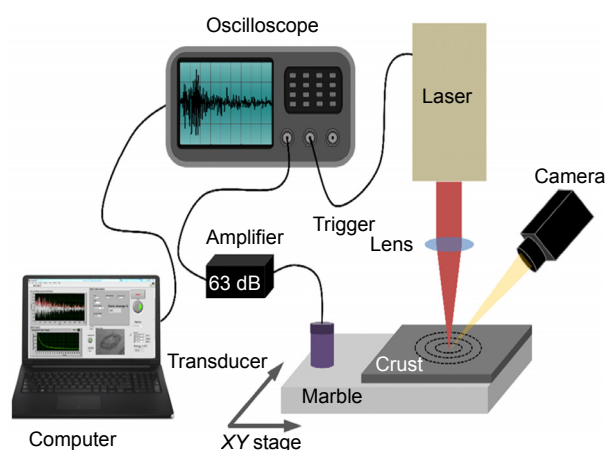


Fig. 1 | Schematic representation of the hybrid photoacoustic and optical experimental apparatus.

A custom-made program was used to record and process the generated PA signal in real time along with the optical images captured by a CMOs Monochromatic Digital camera with resolution of 5M Pixel (iDs, UI-3480CP-M-GL). The camera was equipped with a C-Mount lens (focal length 35 mm – Edmund Optics) in synchronization with the laser trigger. The original PA waveform was recorded for each incident pulse and the average amplitude is obtained following the Hilbert transformation of the respective signal. The waveform was sampled using 1000 points for the selected temporal window (600 μ s or 60 μ s) and the data are saved in txt and xls format. For the statistical analysis and further

signal processing of the data, Matlab programming environment was employed, while the graphs were generated with Origin graphing software.

Irradiation protocol and analytical techniques

The samples were irradiated at a variety of laser parameters using two different wavelengths either individually or simultaneously. The fluence values ranged from 0.1 to 1.0 J/cm² for the 1064 nm and 355 nm, while the simultaneous use of the two beams was investigated for fluence ratios F_{IR}/F_{UV} of 4/1 and 1/1. The number of the laser pulses remained constant (20) in all tests. The thickness of the crust layer, as well as, the depth of the ablated region was measured using a Perthometer S5P (Mahr, Göttingen, Germany) profilometer. Each measurement was repeated 5 times and the results presented correspond to the average calculated values along with their standard deviation.

Results and discussion

Laser cleaning monitoring

In order to monitor the ablation process using the IR wavelength ($F_{IR}=0.8$ J/cm²) and obtain accurate information regarding the cleaning efficiency through the PA signal, the recording temporal window was set at 60 μ s, corresponding to a sampling rate of 16.7 MHz. A post processing analysis protocol of the original waveform (Fig. 2(a)) was established to detect the incident laser pulse that removes the crust, revealing the marble substrate. More specifically, the original PA waveforms generated by each laser pulse ($N=2, 3, 4$ etc.) were cross correlated with the respective waveform resulting from the first incident pulse ($N=1$) (Fig. 2(b)). For every subsequent pulse ($N=2, 3, 4$ etc.) the maximum amplitude of the cross correlation product was extracted as a function of the number of applied pulses (Fig. 2(c)). Furthermore, the absolute value of the percentage change in the maximum amplitude of the cross correlation operation was calculated between subsequent pulses (Fig. 2(d)). This value enabled the precise determination of the incident laser pulse (5th) for which the overlayer was removed from the sample. The decay of the cross correlation amplitude with an increasing pulse number can be mainly attributed to the reduction of the PA amplitude as a result of the material removal, lowering the effective absorption coefficient for the employed irradiation wavelength. Furthermore, structural and photothermal modification of the overlayer has a large impact on the amplitude and phase

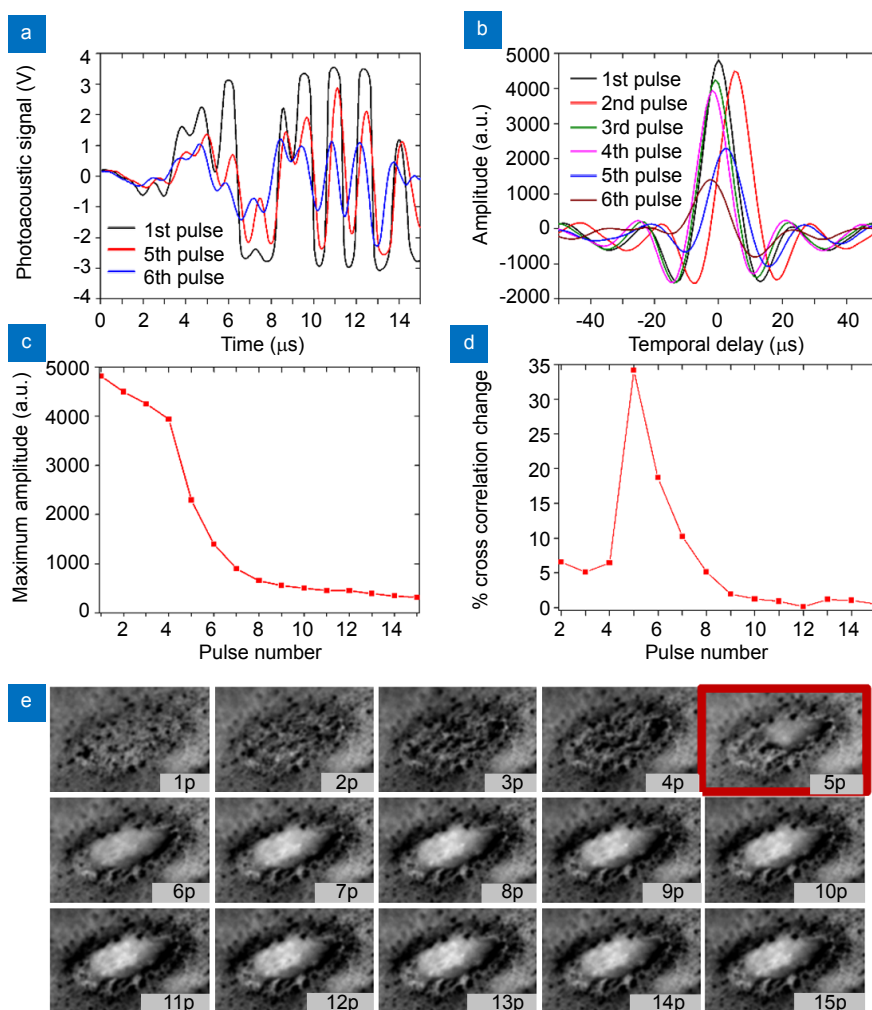


Fig. 2 | (a) Recorded PA waveform for $F_{IR}=0.8 \text{ J/cm}^2$ at 1st, 5th and 6th laser pulse respectively. (b) Cross correlation of PA waveforms generated after the incidence of N th and 1st pulse. (c) Maximum amplitude of cross correlation operation calculated for the first 15 laser pulses. (d) Percentage change of cross correlation maximum amplitude. The peak indicates the pulse at which the marble substrate has been reached. (e) Optical images recorded for the first 15 laser pulses. Red margin indicates the point where the maximum change has been observed according to Fig. 2(d).

of the individual PA frequency components comprising the generated broadband signal, providing thus an altered waveform which differs significantly from the PA waveform recorded on the incidence of the first pulse.

The depth of the crater formed on the marble surface at the end of the irradiation process was measured at $(104.6 \pm 29.8) \mu\text{m}$. The evolution graphs of the cross correlation product and its maximum amplitude (Figs. 2(b) and 2(c)) cannot clearly denote the pulse for which the crust is removed. However, the calculated percentage change presents a well distinguishable peak for the pulse which eliminates the unwanted material (Fig. 2(d)).

Following this signal analysis protocol, three different cleaning regimes were determined, namely: a) the detection of substrate's damage due to the use of high fluence values above the marble's ablation threshold, b) the effi-

cient removal without damage to the substrate (optimum cleaning) and c) inefficient crust removal. These cleaning regimes can be observed in Fig. 3 following irradiation at 1064 nm with fluence values $F = 1.0 \text{ J/cm}^2$, $F = 0.8 \text{ J/cm}^2$ and $F = 0.6 \text{ J/cm}^2$ respectively which have been found to correspond to these three different cleaning levels.

Irradiation with 20 IR pulses at $F = 1.0 \text{ J/cm}^2$ (black lines in Figs. 3(a) and 3(b)) results in damage of the marble's substrate; once the crust has been removed, any further irradiation at relatively high fluence values will cause damage to the marble surface. The crust is removed at the 8th pulse (Fig. 3(c)) and the additional peaks detected correspond to the ablation of the marble and further extraction of material (Fig. 3(d)). Under such overcleaning conditions, the crater depth after 20 incident laser pulses was measured at $(163.2 \pm 32.0) \mu\text{m}$.

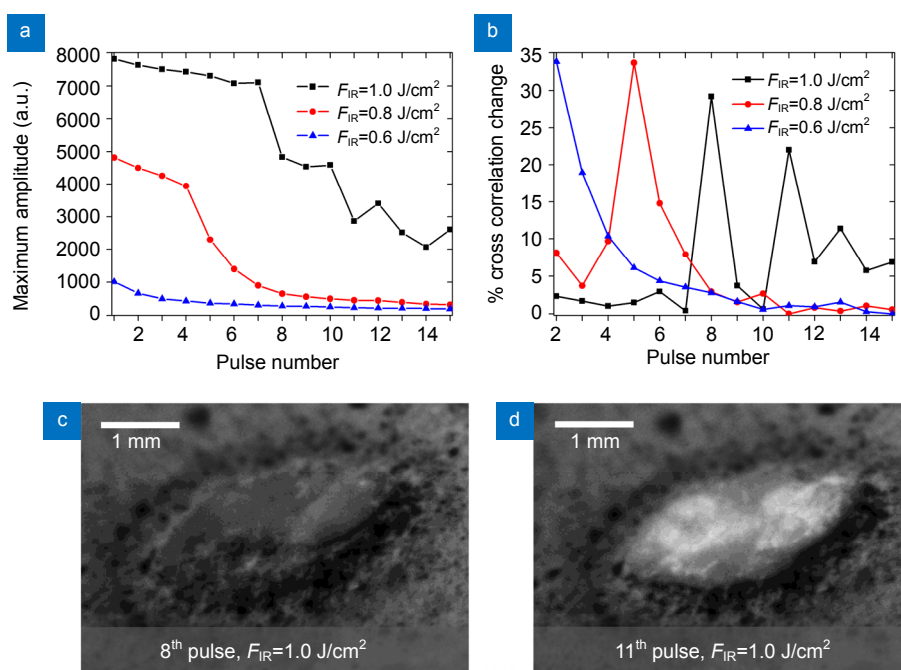


Fig. 3 | (a) Maximum amplitude of cross correlation product for three different fluence values as a function of pulse number. (b) Maximum amplitude percentage change. (c) Optical image corresponding to the 8th laser pulse. (d) Optical image corresponding to the 11th laser pulse. For both cases, irradiation fluence has been equal to 1.0 J/cm^2 .

The irradiation condition of $F = 0.8 \text{ J/cm}^2$ (highlighted with red color in Figs. 3(a) and 3(b)) is considered to be the optimum irradiation condition, where the deposition layer is effectively removed without damage in the marble surface. The unwanted layer is effectively removed at the 5th laser pulse, as can be clearly observed in Fig. 3(b). Subsequent laser pulses do not ablate the marble surface as confirmed by the absence of peaks after the 5th pulse. Finally, the irradiation condition that corresponds to a lower fluence value ($F = 0.6 \text{ J/cm}^2$, denoted with blue color in Figs. 3(a) and 3(b)) is incapable of removing totally the crust. The crater formed is not significant in this case ($55.3 \pm 10.0 \mu\text{m}$) while the absence of peaks in graph of Fig.

3(b) confirms the ineffective cleaning.

A similar signal processing methodology was also adopted for the monitoring of the cleaning progress with 355 nm wavelength, as well as, the simultaneous use of the two wavelengths. A characteristic example is presented in Figs. 4(a) and 4(b), where the deposition material has been removed at the 3rd laser pulse for irradiation with $F_{UV} = 0.5 \text{ J/cm}^2$ without further substrate damage (blue line in Fig. 4(b)). The simultaneous irradiation with $F_{IR}/F_{UV} = 0.8/0.2$ results in damage to the substrate at the 8th laser pulse (black line in Fig. 4(b)), while the ratio $F_{IR}/F_{UV} = 0.4/0.1$ (red line in Fig. 4(b)) does not efficiently remove the unwanted layer, as additionally confirmed by

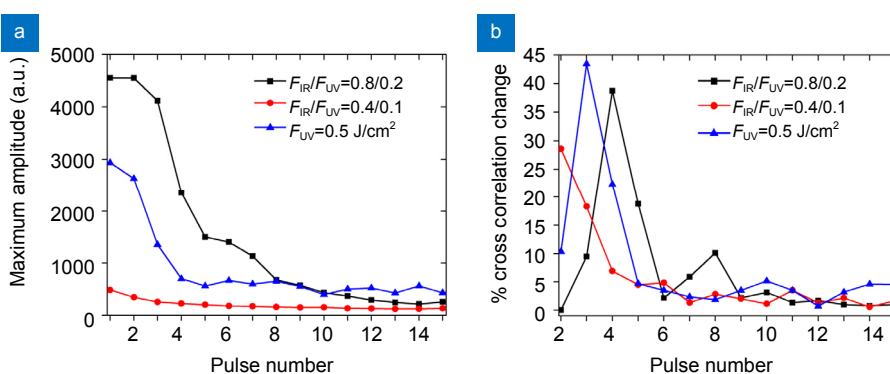


Fig. 4 | (a) Maximum amplitude and (b) Cross correlation maximum amplitude percentage change for irradiation with 355 nm and the simultaneous use of two wavelengths in fluence ratio $F_{IR}/F_{UV} = 4/1$.

the optical images.

Investigation of laser ablation mechanisms

Photoacoustic amplitude as a function of laser fluence

The initial PA pressure rise (p_0) can be expressed as a function of the laser fluence value (F) as $p_0 = \Gamma \eta_{th} \mu_a F$, where Γ is the Grueneisen parameter (dimensionless) defined as $\Gamma = \beta / (\kappa \rho C_v)$, (β is the thermal coefficient of volume expansion, κ the isothermal compressibility, ρ is the mass density and C_v the specific heat capacity), η_{th} is the percentage of pulse energy converted into heat and μ_a the optical absorption coefficient for the employed wavelength³⁸. As can be observed, the intrinsically generated PA signal is directly proportional to the incident laser fluence value, defining the temperature rise of the sample's surface during the irradiation of specific wavelength. However, the PA equation contains temperature dependent parameters such as the thermal coefficient of volume expansion, the specific heat capacity and the isothermal compressibility factor which can introduce nonlinear terms³⁹. A direct measurement of the temperature dependence of these parameters would be beyond the scope of the current study. Nevertheless, the onsets of non-linear behavior, for the purposes of our experiments, were defined through a measurement of the generated PA signal for gradually increasing fluence values. In this manner, the fluence regime, where non-linear temperature dependence is dominant, was defined for both individual wavelengths of 1064 nm and 355 nm.

For the realization of these experiments, the mean PA amplitude was studied for a number of increasing fluence values of both individual wavelengths. In order to ensure the accuracy of the measurements, each point is represented by the average value of the mean PA amplitude from five different spots, while the error bars represent

the standard deviation of the measurements.

The results from these experiments are presented in Fig. 5(a) for the 1064 nm and Fig. 5(b) for the 355 nm wavelength respectively. The colored solid line corresponds to the respective 2nd order polynomial fit of the experimental points, which is characterized by high adjusted R^2 values ($R^2 > 0.99$). These results show that PA signal does not present a linear behavior as a function of fluence F ; instead it is rather described by introducing an additional quadratic term. Despite the apparent non-linear behavior of PA amplitude, it was possible to identify a low fluence regime where the relationship among the PA signal and F is approximately linear.

Initially, the intercept point in both cases has been fixed at 0.03 V (similar to the detection limit of our system) and represents the noise background of acoustic detection. By equalizing the first and second order term of the polynomial equation, it is possible to determine the F value for which the contribution of both linear and non-linear terms becomes comparable. Therefore, we can reasonably assume that for fluence values below this level, the linear term is dominant and the PA signal is approximately proportional to the laser induced temperature rise. Under such conditions, the linear fit of the data has been performed in the fluence regime of 0.1–0.6 J/cm² for the 355 nm and in 0.1–0.5 J/cm² regime for the 1064 nm (black lines in Figs. 5(b) and 5(a)) and is characterized by high R^2 values ($R^2 > 0.99$).

As expected, the upper fluence value of the linear regime is higher for the UV wavelength compared to the IR, given that IR radiation is generally associated with stronger thermal effects and higher temperature rise. The associated laser ablation mechanisms can be investigated in the low fluence regime where F and T present an

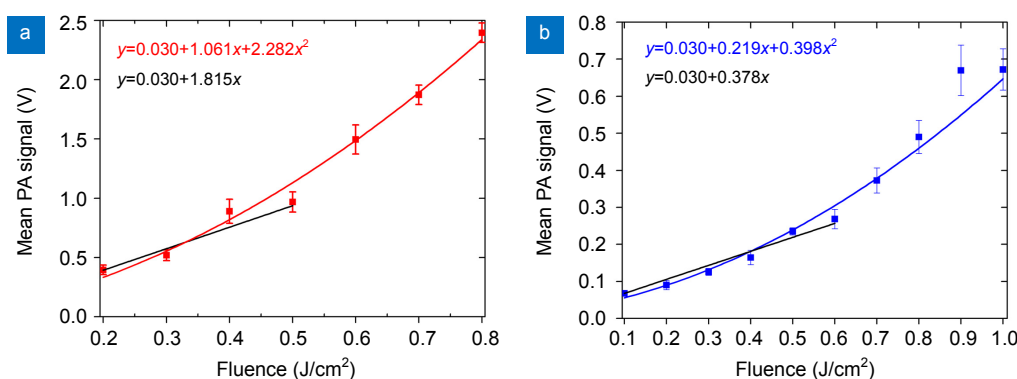


Fig. 5 | Mean PA signal for varying fluence values for the 1064 nm (a) and 355 nm (b) laser beam. The black line corresponds to the polynomial fit of the data, while the blue/red one to the linear fit in the low fluence regime. The error bars represent the standard deviation of five measurements.

approximately linear behavior.

Estimation of relative temperature ratio for IR and UV irradiation

As has already been discussed previously, each laser wavelength induces different ablation mechanisms through which the material is extracted^{8,40}. Assuming that all of the incident laser energy is converted into heat, and with the constrain that the irradiation fluence values are found within the linear PA regime, a calculation/estimation for the ratio of the laser induced temperature is feasible. For thermal and stress confinement conditions³⁸, the pressure rise immediately after the laser pulse is associated with the local temperature rise^{41,42} by the equation $p_0=(\beta/\kappa)T$. Therefore, since β and κ are not considered to be temperature-dependent parameters, the relative ratio of pressure rise (P_{IR}/P_{UV}) is directly proportional to the relative ratio of temperature rise (T_{IR}/T_{UV}). For the realization of these measurements, the transducer was fixed in the corner of the mock-up and a total of 25 pairs of spots were analyzed. Each pair of spots consists of one spot irradiated with 20 pulses of 1064 nm and another one irradiated using 355 nm. The selected fluence value is equal for both wavelengths. In addition, the simultaneous combination of both wavelengths was also investigated using two different fluence ratios with values of $F_{IR} = F_{UV} = 0.25 \text{ J/cm}^2$ and $F_{IR} = 0.40 \text{ J/cm}^2, F_{UV} = 0.10 \text{ J/cm}^2$. The simultaneous ratio value of $F_{IR}/F_{UV} = 4/1$ was investigated because it was the condition selected as optimum for the cleaning of environmental crusts from marble based on the literature⁵. On the other hand, the

$F_{IR}/F_{UV} = 1/1$ has been studied for comparison purposes in order to monitor the signal evolution and investigate the dominant ablation mechanisms during simultaneous irradiation with equal beam contribution.

The initial aim was to study the evolution of the mean PA amplitude of the recorded signal for each wavelength (Fig. 6(a)), along with the optical images of the treated surface (Fig. 6(b)). In Fig. 6(a), the mean PA amplitude (from 25 spots) for irradiation with $F = 0.5 \text{ J/cm}^2$ at 1064 nm and 355 nm and increasing number of pulses is denoted by points. In this figure the solid lines represent an empirical power fit of the data and the error bars correspond to the respective standard deviation of the measurements. The amplitude of the PA signal for the 1064 nm (red color) and 355 nm (blue color) presents a decay for the first incident laser pulses while it reaches a plateau approximately after the 5th pulse. Using a statistical analysis protocol developed in Matlab environment, an empirical power fitting of the data was performed using the method of nonlinear least squares ($y=ax^{-b}$, where x is the pulse number and y the PA signal). The results presented hereafter represent their average values, while the fitting was characterized by high adjusted R^2 values, confirming the suitability of the selected model (Table 1). Irradiation with IR at 1064 nm results into a rapid signal decay during the first three pulses (Fig. 6(a)), whereas irradiation with 355 nm appeared to result in a more gradual reduction of the PA signal.

The temperature ratio was calculated by the 1st incident pulse to the mock-up, which is essentially interacting

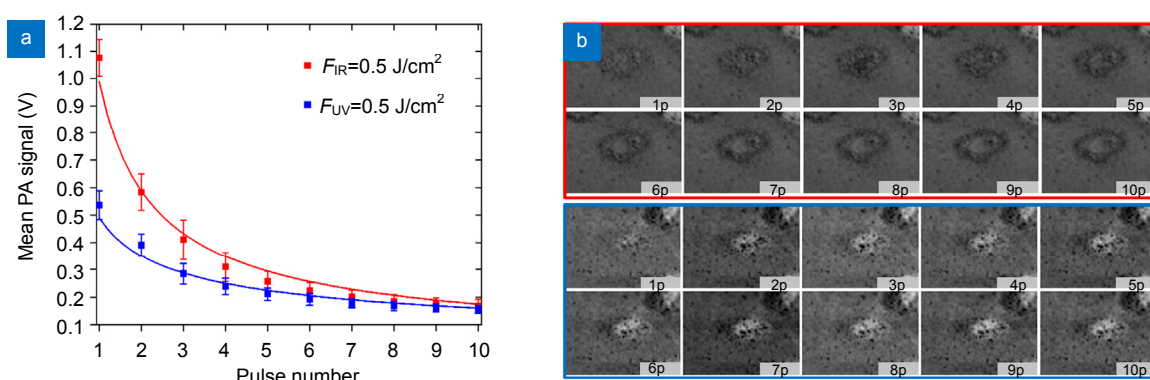


Fig. 6 | (a) Mean PA signal recorded from 26 spots irradiated with $F_{UV} = F_{IR} = 0.5 \text{ J/cm}^2$ along with **(b)** Characteristic optical images corresponding to 10 incident laser pulses of IR (red margin) and UV (blue margin) radiation.

Table 1 | Empirical fitting of PA data for different fluence ratios.

Fitting model: $y=ax^{-b}$	F_{IR}	F_{UV}	$F_{IR}/F_{UV}=4/1$	$F_{IR}/F_{UV}=1/1$
b	0.88 ± 0.14	0.57 ± 0.05	0.72 ± 0.09	0.65 ± 0.07
a	1.10 ± 0.24	0.54 ± 0.07	0.49 ± 0.07	0.45 ± 0.06
R^2	>0.99	>0.98	>0.98	>0.98

Table 2 | 1st pulse PA amplitude values for various irradiation conditions.

	F_{IR}	F_{UV}	$F_{IR}/F_{UV}=4/1$	$F_{IR}/F_{UV}=1/1$
PA amplitude of 1 st pulse	1.07 ± 0.06 V	0.53 ± 0.05 V	0.54 ± 0.05	0.48 ± 0.04
% Δ (1 st – 2 nd pulse)	$45.5\% \pm 4.9\%$	$26.8\% \pm 5.0\%$	$43.2\% \pm 3.1\%$	$38.4\% \pm 5.1\%$
1 st pulse P_{IR}/P_{UV}	2.05 ± 0.21	-		

with the original material, because subsequent pulses encounter a material with modified/alterd physico-chemical properties (color, absorption, etc.). Results from these measurements, performed with $F = 0.5$ J/cm² for both individual wavelengths, are presented in Table 2. The PA amplitude recorded for the 1st pulse during IR ablation is approximately twice the one recorded for the UV wavelength (Fig. 6(a); Table 2). Through the statistical analysis performed, the mean PA signal for the 1st IR pulse has been calculated to be 1.07 V \pm 0.06 V and the mean PA for the 1st UV pulse 0.53 V \pm 0.05 V. Comparing the mean PA signals recorded for the analyzed pairs of spots after the 1st pulse irradiation it was found that $PA_{IR}/PA_{UV}=2.05 \pm 0.21$. This is an indication that the temperature rise during the ablation with IR is two times higher than that in the UV. Consequently, this result confirms the knowledge that different ablation mechanisms are induced by each individual wavelength; the use of 1064 nm results in more intense thermal effects in comparison to the 355 nm.

Regarding the simultaneous use of the two wavelengths, it was found that the signal evolution depends significantly on the fluence ratio. The mean normalized PA signal corresponding to 25 spots irradiated with the two wavelengths individually and their simultaneous combination is presented in Fig. 7. The PA signal has been normalized to the maximum value for comparison purposes.

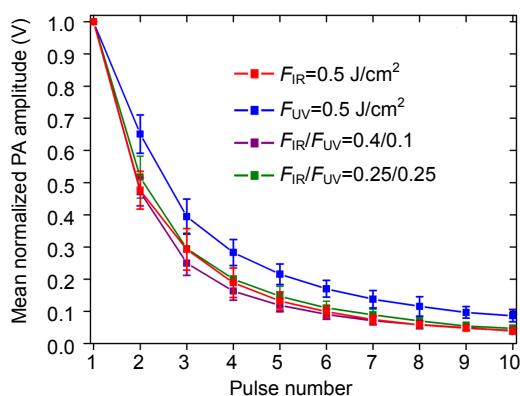


Fig. 7 | Mean normalized PA signal for 10 incident laser pulses of: $F_{IR} = 0.5$ J/cm² (red), $F_{UV} = 0.5$ J/cm² (blue), simultaneous $F_{IR} = 0.4$ J/cm² and $F_{UV} = 0.1$ J/cm² (purple), simultaneous $F_{IR} = F_{UV} = 0.25$ J/cm² (green).

Comparing the single-wavelength to simultaneous IR and UV irradiation, the normalized PA signals are closely dependent on the relative contribution of each beam. Simultaneous irradiation with fluence ratio $F_{IR}/F_{UV}=0.4/0.1$ resulted in similar outcome with the IR laser ablation, which can be explained due to the high proportion of the IR laser beam in comparison to the UV. The 1/1 fluence ratio exhibits slightly lower results, indicating that it is less efficient in the material removal in comparison to the 4/1 ratio.

Conclusions

In summary, we have developed a hybrid photoacoustic and optical system for the in-situ and real-time monitoring of laser cleaning and the investigation of the laser ablation mechanisms that dominate the cleaning with IR and UV laser wavelengths. We also introduced a successful and novel photoacoustic data processing protocol which can be used to indicate the incident pulse that eliminates the crust layer, using only the generated waveform from the interaction of the laser beam with the material. So far, we have demonstrated the potential of the system for the monitoring of laser cleaning with IR and UV wavelengths, both individually and simultaneously in a variety of fluence values. We compared the generated PA signal from the two different wavelengths and associated it with the laser ablation mechanisms, confirming the models supporting the domination of photothermal mechanisms during IR irradiation. In addition, we calculated the ratio of the relative temperatures that are induced upon IR and UV laser ablation, which for our studies on marble slabs covered with simulated thin pollution crust was calculated to be $T_{IR}/T_{UV} \sim 2$. A compact set-up dedicated to PA analysis and monitoring of conservation interventions is our subsequent task, while the application of the photoacoustic technique for the elucidation of the laser cleaning mechanisms has been considered for the first time.

This prototype system is planned to be tested for the monitoring of laser cleaning on real objects, while in the future we are planning to integrate non-contact transducers in the monitoring experimental setup. This will

increase the system portability and will allow the accurate implementation of the technique in samples with variable surface geometries. The use of such detectors can also allow the monitoring of cleaning procedures in objects with fragile and delicate surfaces, where non-contact monitoring methodologies are required. In addition, developments in the software are planned to be performed in order to monitor the cleaning progress of larger areas, during cleaning procedures performed using an automated scanning system. In the case of an automated cleaning procedure, the maximum cross correlation amplitude change values could be employed to regulate the incident number of laser pulses released on the sample according to the local thickness of the crust and the irregularities of the surface morphology. Such highly promising capabilities would highlight further the potential of the developed hybrid system as regards the reliable on-line monitoring of various laser cleaning interventions.

References

- Cooper M. *Laser Cleaning in Conservation: An Introduction* (Butterworth Heinemann, Oxford, 1998).
- Fotakis C, Anglos D, Zafirooulos V, Georgiou S, Tornari V. *Lasers in the Preservation of Cultural Heritage: Principles and Applications* (CRC Press, Boca Raton, 2006).
- Siano S, Agresti J, Cacciari I, Ciofini D, Mascalchi M et al. Laser cleaning in conservation of stone, metal, and painted artifacts: State of the art and new insights on the use of the Nd:YAG lasers. *Appl Phys A* **106**, 419–446 (2012).
- Pouli P, Oujja M, Castillejo M. Practical issues in laser cleaning of stone and painted artefacts: optimisation procedures and side effects. *Appl Phys A* **106**, 447–464 (2012).
- Pouli P, Papakonstantinou E, Frantzikinaki K, Panou A, Frantzi G et al. The two-wavelength laser cleaning methodology; theoretical background and examples from its application on CH objects and monuments with emphasis to the Athens Acropolis sculptures. *Herit Sci* **4**, 9 (2016).
- Maravelaki P V, Zafirooulos V, Kilikoglou V, Kalaitzaki M, Fotakis C. Laser-induced breakdown spectroscopy as a diagnostic technique for the laser cleaning of marble. *Spectrochim Acta Part B: At Spectrosc* **52**, 41–53 (1997).
- Gobernado-Mitre I, Prieto A C, Zafirooulos V, Spetsidou Y, Fotakis C. On-line monitoring of laser cleaning of limestone by laser-induced breakdown spectroscopy and laser-induced fluorescence. *Appl Spectrosc* **51**, 1125–1129 (1997).
- Salimbeni R, Pini R, Siano S. Achievement of optimum laser cleaning in the restoration of artworks: expected improvements by on-line optical diagnostics. *Spectrochim Acta Part B: At Spectrosc* **56**, 877–885 (2001).
- Melessanaki K, Stringari C, Fotakis C, Anglos D. Laser cleaning and spectroscopy: a synergistic approach in the conservation of a modern painting. *Laser Chem* **2006**, 42709 (2006).
- Fortes F J, Cabalin L M, Laserna J J. The potential of laser-induced breakdown spectrometry for real time monitoring the laser cleaning of archaeometallurgical objects. *Spectrochim Acta Part B: At Spectrosc* **63**, 1191–1197 (2008).
- Ciofini D, Oujja M, Cañamares M V, Siano S, Castillejo M. Spectroscopic assessment of the UV laser removal of varnishes from painted surfaces. *Microchem J* **124**, 792–803 (2016).
- Moretti P, Iwanicka M, Melessanaki K, Dimitroulaki E, Kokkinaki O et al. Laser cleaning of paintings: in situ optimization of operative parameters through non-invasive assessment by optical coherence tomography (OCT), reflection FT-IR spectroscopy and laser induced fluorescence spectroscopy (LIF). *Herit Sci* **7**, 44 (2019).
- Fischer C, Kakoulli I. Multispectral and hyperspectral imaging technologies in conservation: current research and potential applications. *Rev Conserv* **7**, 3–16 (2006).
- Papadakis V, Loukaiti A, Pouli P. A spectral imaging methodology for determining on-line the optimum cleaning level of stonework. *J Cult Herit* **11**, 325–328 (2010).
- Pozo-Antonio J S, Fiorucci M P, Ramil A, Rivas T, López A J. Hyperspectral imaging as a non destructive technique to control the laser cleaning of graffiti on granite. *J Nondestr Eval* **35**, 44 (2016).
- Klemm A J, Sanjeevan P. Application of laser speckle analysis for the assessment of cementitious surfaces subjected to laser cleaning. *Appl Surf Sci* **254**, 2642–2649 (2008).
- Bernikola E, Melessanaki K, Hatzigiannakis K, Pouli P, Tornari V. Real-time monitoring of laser assisted removal of shellac from wooden artefacts using Digital Holographic Speckle Pattern Interferometry. In *Lasers in the Conservation of Artworks* 52–59 (Archetype Publications Ltd, London, 2013).
- Márton Z, Kisapáti I, Török Á, Tornari V, Bernikola E et al. Holographic testing of possible mechanical effects of laser cleaning on the structure of model fresco samples. *NDT E Int* **63**, 53–59 (2014).
- Iwanicka M, Musiela J, Łukaszewicz J W, Stoksik H, Sylwestrzak M. The potential of OCT for assessing laser assisted removal of deposits from ceramic tiles. In *Lasers in the conservation of artworks XI. Proceedings of the International Conference LACONA XI 2016* 105–114 (NCU Press, 2017); <http://doi.org/10.12775/3875-4.07>.
- Striova J, Fontana R, Barucci M, Felici A, Marconi E et al. Optical devices provide unprecedented insights into the laser cleaning of calcium oxalate layers. *Microchem J* **124**, 331–337 (2016).
- Tserevelakis G J, Siozos P, Papanikolaou A, Melessanaki K, Zacharakis G. Non-invasive photoacoustic detection of hidden underdrawings in paintings using air-coupled transducers. *Ultrasonics* **98**, 94–98 (2019).
- Cooper M I, Emmony D C, Larson J. Characterization of laser cleaning of limestone. *Opt Laser Technol* **27**, 69–73 (1995).
- Lee J M, Watkins K G. In-process monitoring techniques for laser cleaning. *Opt Lasers Eng* **34**, 429–442 (2000).
- Bregar V B, Možina J. Photoacoustic analysis of the laser-cleaning process. *Appl Surf Sci* **185**, 277–288 (2002).
- Jankowska M, Śliwiński G. Acoustic monitoring for the laser cleaning of sandstone. *J Cult Herit* **4**, 65–71 (2003).
- Gómez C, Costela A, García-Moreno I, Sastre R. Comparative study between IR and UV laser radiation applied to the removal of graffiti on urban buildings. *Appl Surf Sci* **252**, 2782–2793 (2006).
- Villarreal-Villela A E, Cabrera L P. Monitoring the laser ablation process of paint layers by PILA technique. *Open J Appl Sci* **6**,

- 626–635 (2016).
28. Tserevelakis G J, Pozo-Antonio J S, Siozos P, Rivas T, Pouli P et al. On-line photoacoustic monitoring of laser cleaning on stone: Evaluation of cleaning effectiveness and detection of potential damage to the substrate. *J Cult Herit* **35**, 108–115 (2019).
 29. Maravelaki-Kalaitzaki P. Black crusts and patinas on Pentelic marble from the Parthenon and Erechtheum (Acropolis, Athens): Characterization and origin. *Anal Chim Acta* **532**, 187–198 (2005).
 30. Potgieter-Vermaak S S, Godoi R H M, van Grieken R, Potgieter J H, Oujja M et al. Micro-structural characterization of black crust and laser cleaning of building stones by micro-Raman and SEM techniques. *Spectrochim Acta Part A: Mol Biomol Spectrosc* **61**, 2460–2467 (2005).
 31. Vergès-Belmin V, Dignard C. Laser yellowing: myth or reality? *J Cult Herit* **4**, 238–244 (2003).
 32. Klein S, Fekrsanati F, Hildenhagen J, Dickmann K, Uphoff H et al. Discoloration of marble during laser cleaning by Nd:YAG laser wavelengths. *Appl Surf Sci* **171**, 242–251 (2001).
 33. Gaviño M, Castillejo M, Vergès-Belmin V, Nowik W, Oujja M et al. Black crusts removal: the effect of stone yellowing and clearing strategies. Air Pollution and Cultural Heritage Leiden: AA Balkema, 239–245 (2004).
 34. Zafirooulos V, Pouli P, Kylikoglou V, Maravelaki-Kalaitzaki P, Luk'yanchuk B S et al. Synchronous use of IR and UV laser pulses in the removal of encrustation: mechanistic aspects, discoloration phenomena and benefits. In *Lasers in the Conservation of Artworks*, 311–318 (Springer, Berlin, Heidelberg, 2005).
 35. Pouli P, Fotakis C, Hermosin B, Saiz-Jimenez C, Domingo C et al. The laser-induced discoloration of stonework; a comparative study on its origins and remedies. *Spectrochim Acta Part A: Mol Biomol Spectrosc* **71**, 932–945 (2008).
 36. Godet M, Vergès-Belmin V, Gauquelin N, Saheb M, Monnier J et al. Nanoscale investigation by TEM and STEM-EELS of the laser induced yellowing. *Micron* **115**, 25–31 (2018).
 37. Papanikolaou A, Siozos P, Philippidis A, Melessanaki K, Pouli P. Towards the understanding of the two wavelength laser cleaning in avoiding yellowing on stonework: a micro-Raman and LIBS study. In *Lasers in the Conservation of Artworks XI, Proceedings of the International Conference LACONA XI* 95–104 (NCU Press, 2017); <http://doi.org/10.12775/3875-4.06>.
 38. Wang L V, Wu H I. *Biomedical Optics: Principles and Imaging* (Wiley, Hoboken, NJ, USA, 2007).
 39. Simandoux O, Prost A, Gateau J, Bossy E. Influence of nanoscale temperature rises on photoacoustic generation: discrimination between optical absorbers based on thermal non-linearity at high frequency. *Photoacoustics* **3**, 20–25 (2015).
 40. Marla D, Bhandarkar U V, Joshi S S. A model of laser ablation with temperature-dependent material properties, vaporization, phase explosion and plasma shielding. *Appl Phys A* **116**, 273–285 (2014).
 41. Feng X H, Gao F, Xu C Y, Li G M, Zheng Y J. Self temperature regulation of photothermal therapy by laser-shared photoacoustic feedback. *Opt Lett* **40**, 4492–4495 (2015).
 42. Feng X H, Gao F, Zheng Y J. Photoacoustic-based-close-loop temperature control for nanoparticle hyperthermia. *IEEE Trans Biomed Eng* **62**, 1728–1737 (2015).

Acknowledgements

This research was supported by the projects a) “POLITEIA II” (Politismos-Technologia, New Technologies in the Research, Study, Documentation and Access to the Information for Cultural Heritage Objects and Monuments II) (MIS 5002478) (implemented under the “Action for the Strategic Development on the Research and Technological Sector”) and b) “HELLAS-CH” (MIS 5002735) (implemented under the “Action for Strengthening Research and Innovation Infrastructures”), both funded by the Operational Programme “Competitiveness, Entrepreneurship and Innovation” (NSRF 2014-2020) and co-financed by Greece and the European Union (European Regional Development Fund). G.J.T acknowledges the financial support of the Stavros Niarchos Foundation within the framework of the project ARCHERS (“Advancing Young Researchers’ Human Capital in Cutting Edge Technologies in the Preservation of Cultural Heritage and the Tackling of Societal Challenges”).

Author contributions

A. P., G. J. T. and P. P. conceived the concept and designed the experiments. K. M. prepared the mock-up samples. A. P. and G. J. T. developed the experimental setup, performed the photoacoustic measurements and analyzed the data. A. P., and G. J. T. wrote the manuscript. P. P., G. Z. and C. F. oversaw all research phases while P. P. and G. Z. contributed significantly to the refinement of the article. P. P. coordinated all phases of the study. All authors commented on the manuscript.

Competing interests

The authors declare no competing financial interests.